Available online at www.sciencedirect.com

SciVerse ScienceDirect

Acta Materialia 61 (2013) 205–216

Acta MATERIALIA

www.elsevier.com/locate/actamat

Inter- and intragranular plasticity mechanisms in ultrafine-grained Al thin films: An in situ TEM study

F. Mompiou [a,*], M. Legros [a], A. Boé [d], M. Coulombier [b], J.-P. Raskin [c], T. Pardoen [b]

[a] CEMES-CNRS and Université de Toulouse, 29, rue J. Marvig, 31055 Toulouse, France
[b] Institute of Mechanics, Materials and Civil Engineering, Université catholique de Louvain, Place Sainte Barbe 2, B-1348 Louvain-la-Neuve, Belgium
[c] Information and Communications Technologies, Electronics and Applied Mathematics (ICTEAM), Microwave Laboratory, Université catholique de Louvain, B-1348 Louvain-la-Neuve, Belgium
[d] Institut d'Electronique, de Microélectronique et de Nanotechnologie (IEMN) UMR CNRS 8520, and Institut de Recherche sur les Composants logiciels et matriels pour l'Information et la Communication Avancé (IRCICA) USR CNRS 3380, Universit Lille 1, 59650 Villeneuve d'Ascq, France

Received 20 July 2012; received in revised form 14 September 2012; accepted 18 September 2012
Available online 15 October 2012

Abstract

The nature of the elementary deformation mechanisms in small-grained metals has been the subject of numerous recent studies. In the submicron range, mechanisms other than intragranular dislocation mechanisms, such as grain boundary (GB)-based mechanisms, are active and can explain the deviations from the Hall–Petch law. Here, we report observations performed during in situ transmission electron microscopy (TEM) tensile tests on initially dislocation-free Al thin films with a mean grain size around 250 nm prepared by microfabrication techniques. Intergranular plasticity is activated at the onset of plasticity. It consists of the motion of dislocations in the GB plane irrespective of the GB character. Surface imperfections, such as GB grooves, are supposed to trigger intergranular plasticity. At larger deformations, the motion of the intergranular dislocations leads to GB sliding and eventually cavitation. In the meantime, GB stress-assisted migration and dislocation emission inside the grain from GB sources have also been observed. The observation of these different mechanisms during the deformation provides an important insight into the understanding of the mechanical properties of metallic thin films.

Keywords: Grain boundary; In situ TEM; Dislocations; Plasticity; MEMS

1. Introduction

The origin of the strength increase accompanying a reduction in grain size has been a longstanding and recurrent question in mechanical metallurgy. Hall and Petch were the first to formulate this finding by the now well-known phenomenological law: $\sigma_y = \sigma_0 + kd^{-1/2}$, where σ_y is the flow stress, d is the grain size and σ_0 and k are hardening constants [1,2]. In the last two decades, with the improvement of processing methods, especially various sorts of severe plastic deformation [3] and electrodeposition methods [4,5], it has become possible to test the validity of the Hall–Petch law down to the nanometer scale. All the experimental data indicate that the linear increase in the flow stress with the negative square root of grain size is no longer valid below 100 nm [4,6,7]. This change in behavior is frequently attributed to a change in the deformation mechanism: in coarse-grained metals, the plastic deformation is controlled by intragranular mechanisms, while in very small grains, grain boundary (GB)-mediated mechanisms are promoted. However, it is not clear (i) what kind of intragranular elementary processes are active just above the Hall–Petch breakdown, (ii) why they are shut down and (iii) what kind of elementary GB processes are favored. Several mechanisms can potentially be active and the

* Corresponding author.
E-mail address: mompiou@cemes.fr (F. Mompiou).

1359-6454/$36.00 © 2012 Acta Materialia Inc. Published by Elsevier Ltd. All rights reserved.
http://dx.doi.org/10.1016/j.actamat.2012.09.051

resulting competition or synergy leading to one or several dominant deformation modes ultimately depends on the material and on minute details of the composition and microstructure.

The first question has been the subject of numerous models based on dislocation theory (see the review in Ref. [8] for instance). All these theories require the existence of sources emitting lattice dislocations in the grain interior and are based on the interaction of dislocations with GBs. The flow stress depends on an internal length scale that is usually related to the dislocation mean free path in work-hardening theories [9–11] and in strain gradient plasticity theories [12–14], or to the length of a pile-up in pile-up models [1,2]. Although the grain size dependence in the Hall–Petch law naturally emerges from these theories, the proportionality factor k is difficult to predict, mainly because it is strongly dependent on the structure of the GB [8]. Dislocation–GB interactions are unfortunately not sufficiently documented and the strength of GBs are then difficult to estimate.

The second point is connected to the breakdown of the pile-up strength when only a very limited number of dislocations is involved [15] or when the internal length scale is of the order of the grain size in strain gradient plasticity-based models [16,17]. However, this explanation is not satisfactory for very small grains where the existence of internal dislocation sources is questionable. For this reason, several authors have suggested, based on molecular dynamics simulations, that GB dislocation sources can be activated in nanograins [18]. Only a small amount of indirect evidence of dislocation emission from GBs in coarse-grained metals exists [19] and the details of the dislocation nucleation mechanisms remain unclear. Moreover it is difficult to distinguish a dislocation source located in or close to a GB or if dislocation nucleation results in stress concentration in a nearby region of a dislocation pile-up.

The third point has received major attention in the last years, since the identification of a number of GB mechanisms: mechanical twinning [20], GB sliding [21] and GB rotation [22]. A growing number of studies have also reported stress-assisted grain growth as an efficient mechanism to accommodate plastic deformation in small-grained materials [23–30]. One of the key question concerns the detailed mechanism allowing GB sliding or shear coupled GB migration and the conditions, i.e. misorientation, orientation of the GB plane with respect to the tensile axis, that can favor one of these mechanisms.

The transition between intragranular and intergranular deformation mechanism is not supposed to be abrupt, and ultrafine-grained (UFG) metals with a grain size ranging between 100 nm and 1 μm appear as ideal candidates to investigate these two types of mechanisms. For several years, in situ transmission electron microscopy (TEM) has appeared to a well-suited tool for probing the elementary deformation mechanisms in small-grained materials [31]. Several studies so far have investigated the interaction between dislocations and GBs [32–34] and dislocation transmission [35,36]. In a previous study on UFG Al prepared by equal-channel angular processing [37], the emission of dislocations from internal sources piling against GBs has been observed. Their reversible motion towards the source when the sample was unloaded explains the inelastic response of the material during microyielding experiments [38]. It has been shown that GBs can act as dislocation sinks in which their stress field can spread [39]. However, because grains were sufficiently large and contained dislocation sources, no intergranular plasticity has been observed. A better understanding of these mechanisms is not only of fundamental interest, but has also an impact on the design of technologies involving small grain size metallic materials. For instance, the use of thin metallic films with grain size in the range between 50 and 500 nm is ubiquitous in a variety of microelectronics, coatings, microelectromechanical systems (MEMS), or stretchable electronics applications. These films are often subject to significant mechanical loads from internal stress or external perturbations,originating, for example, from thermal expansion mismatch with the substrate [40]. The details of the aforementioned relaxation mechanisms directly control the ductility, strength, creep and fracture properties. These properties must be controlled or adapted to the working conditions, whether it is a flexible electronic device in which the metallic lines must survive large strains, MEMS microbridges which must sustain high stresses without permanent bending, or thin coatings which must not scratch under mechanical loading to preserve functionality.

The goal of this study is to investigate the deformation mechanisms in initially ultrafine dislocation-free Al grains. Metallic thin films constitute ideal candidates for this purpose as they can be grown with few defects, unlike material produced by severe plastic deformation processes. Because freestanding films are difficult to manipulate, lithography-based techniques were used to fabricate a MEMS-type device embedding freestanding structures suitable for TEM micro-testing experiments. After a short presentation of the experimental set-up and of the initial thin film microstructure, we will describe the observations of plasticity mechanisms and discuss the results. Attention will be focused on the unexpected observation of a frequent occurrence of GB dislocation glide at small strains, independent of the GB character. This intergranular plasticity mechanism is followed at larger strains by intragranular plasticity, accompanied by some GB migration and damage accumulation at GBs.

2. Experimental

The in situ test structures were produced using microfabrication techniques based on MEMS-type procedures, closely resembling the technique presented in Ref. [41,42]. These structures are schematically shown in Fig. 1. The handling substrate is a 200 μm thick, 3 in. single-crystal silicon wafer. The fabrication involves two-layer depositions of sacrificial and specimen layers. The sacrificial layer is

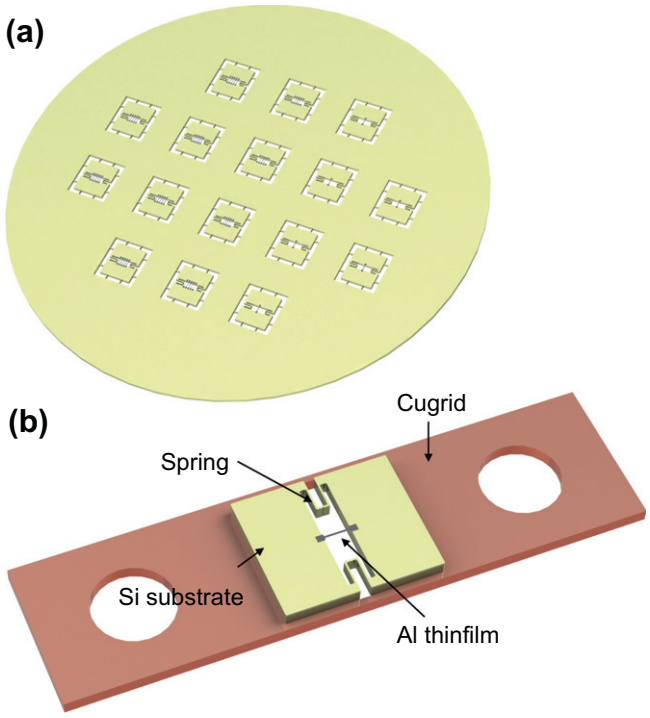

Fig. 1. (a) An assembly of microtest structures on their silicon wafer. (b) An individual MEMS removed from the wafer and glued to a copper grid for in situ tensile tests along the thin film long axis. Lateral silicon springs allow an easy manipulation and enable elongation of the film during the tensile test.

made of a 1 μm thick plasma-enhanced chemical vapor deposited SiO_2 layer deposited at 300 °C using SiH_4 (diluted in N_2O/N_2) as precursor (with gas flow respectively equal to 100/700/1000 sccm). The specimen layer is made of a 300 nm thick 99.999% pure Al film deposited by evaporation at room temperature. Photolithography and dry etching with a Cl_2/CCl_4 plasma are used to pattern the specimen layer. The next step is the patterning of the substrate, which serves three goals: the creation of a window under the specimens to enable TEM observations (i.e. cavities under specimen beams); the fabrication of springs; and the precutting of the samples to make it easier to separate the chip from the wafer. A 5 μm thick photoresist (SPR 220) is spin-coated and patterned by photolithography to act as a mask on the back side of the wafer. Then, the silicon wafer is etched from the back using a modified Bosch process. The thick SiO_2 sacrificial layer acts as an etch-stop layer and an over-etch time must thus be used to avoid incomplete removal of the silicon substrate due to variations of substrate thickness over the entire wafer and due to the etch rate dependence on the cavity size. Finally, the photoresist layer is removed. At this point, the Al specimens are still not freestanding. Wet etching of the sacrificial layer in 73% fluoridric acid (HF) is performed, followed by rinsing in isopropanol (IPA).

Individual microtest structures were then detached from the Si handling structure by cutting mechanically the Si bridges that retain the microtest structures to the Si wafer (Fig. 1a). Each microtest structure carries one or several parallel 150 μm long and 8 μm large dogbone-shaped thin films. Microtest structures were then glued to a copper grid for mounting in a GATAN room-temperature straining holder (Fig. 1b). The two lateral springs on the microtest structure facilitate the manipulation without breaking the films during transfer from the wafer to the grid. They also allow the films to elongate and deform during the in situ test. The in situ tensile tests were then run in a JEOL 2010HC operated at 200 kV by applying a controlled displacement to the grid along an axis parallel to the film length. Video sequences were recorded by a MEGAVIEW III camera at 25 fps on a DVD recorder. The strain was evaluated by measuring the evolution of the gauge length of individual films. Automated crystal orientation mappings (ACOM) were obtained by the ASTAR system operating on a CM20FEG. Microstructural characterization was performed using TSL-EDAX software.

3. Results

3.1. Initial microstructure

A typical orientation map obtained by ACOM in the transmission electron microscope before straining is shown in Fig. 2a. The microstructure consists of equiaxed UFG grains with a mean grain size of around 250 nm (Fig. 2d) involving a small proportion of grains larger than 500 nm. Because the film thickness is about 300 nm, the film contains, for most of the volume, only one grain over the thickness. Fig. 2c shows a strong {1 1 1} texture perpendicular to the film. Most of the grains exhibit GBs perpendicular to the film plane, indicating a columnar growth. The texture is the result of surface energy minimization during grain growth in the film, while the columnar structure is due to continuous grain growth during film thickening [43]. This has been demonstrated by Lita et al. [44] in sputtered Al films. These authors found that the grain size follows a log-normal distribution of grain size spreads around the law $d = 0.8h^{0.9}$, where d is the mean grain size and h the film thickness in microns. Taking $h = 0.3$ μm leads to $d = 0.27$ μm which is in close agreement with the present observations. The fraction of larger grains can be attributed to abnormal grain growth due to the presence of impurities that prevent normal grain growth during thickening. Fig. 2b highlights the GBs according to their type: in blue, high-angle GBs (HAGBs); in red, coincident site kattice GBs (CSL GBs); and, in green, low-angle GBs (LAGBs). The distinction between HAGBs and LAGBs corresponds to a minimum misorientation larger than 15° [45]. Among all the GBs, 75% are HAGBs, 10% LAGBs and 15% are CSL GBs with a majority of Σ3. No dislocation has been observed prior to deformation. Interestingly, a concentration of 1.5 at.% fluor, probably originating from the etching process, was also found homogenously distributed in the microstructure.

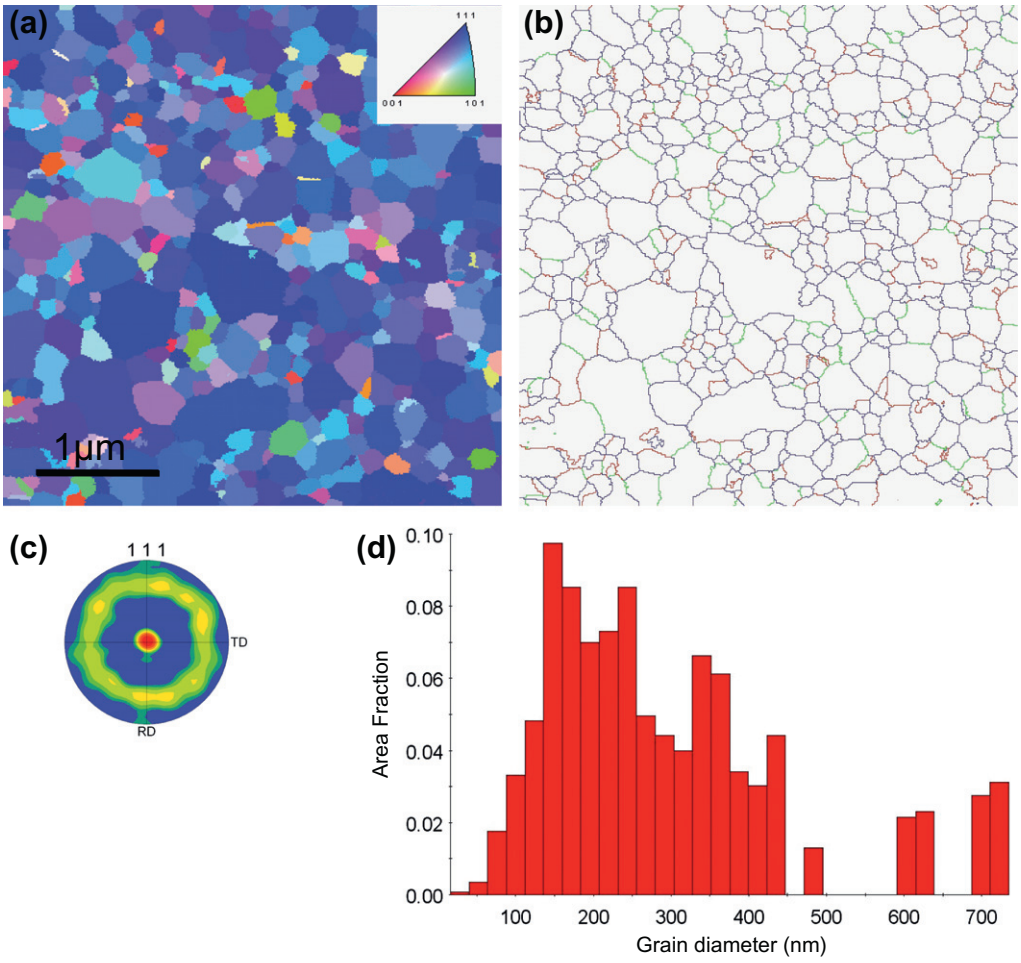

Fig. 2. TEM automatic crystal orientation mapping (ACOM) of a 4 × 4 μm unstrained film section: (a) color map showing the different grain orientations; (b) traces of the GBs according to their type: in blue, high-angle GBs (HAGBs); in red, coincident site lattice GBs (CSL GBs); and, in green, low-angle GBs (LAGBs); (c) pole figure and (d) corresponding histogram of grain size distribution. (For interpretation of the references to color in this figure legend, the reader is referred to the web version of this article.)

3.2. Intergranular plasticity regime

The first deformation events involving movement of defects have been detected below 2% imposed deformation. Unexpectedly, these events essentially consist of dislocation glide inside GBs. Fig. 3 is composed of bright-field (BF) images extracted from a video sequence at different times, and shows the nucleation and the motion of dislocations in the GB between grain *G*1 and *G*2, noted *GB*12 in the following. Electron diffraction patterns taken during the in situ straining experiments under different inclinations were used to determine the orientations of two adjacent grains and thus to characterize the GB.

The *G*12 corresponds here to a HAGB $[19\overline{1}3]$ 53°. Because the film is tilted by 26° around the straining axis (noted *T* in Fig. 3a), the GB is seen inclined, exhibiting a classic fringe contrast. A dislocation, noted d_1, is seen in the GB. Upon straining, a second dislocation, noted d_2, is nucleated close to the triple junction (TJ) between *G*1, *G*2 and *G*3 (noted in the following *TJ*123) (Fig. 3b). Fig. 3e is a schematic of the geometry of the triple junction. When the stress gets large enough, the dislocation d_2 expands in the GB while the dislocation d_1 remains trapped near the surface, probably blocked by the native oxide layer (Fig. 3c). However, it can be noted that the contrast of d_1 decreases between $t = 0.2s$ (Fig. 3b) and $t = 2.2s$ (Fig. 3c), whereas the dislocation has almost disappeared at $t = 59s$ (Fig. 3d). This effect is typical of the spreading of the dislocation stress–strain field in an interface, presumably here an amorphous alumina layer, where the Burgers vector cannot decompose [38,39]. The spreading is thus supposed to occur by atomic rearrangements which are thermally activated, and hence progressive. The contrast of the dislocation d_2 decreases gradually for the same reason. When the dislocation d_2 moves inside the GB, it is temporarily pinned at certain obstacles (marked by arrows in Fig. 3d) that cannot be resolved at this length scale. These obstacles might be due to a solute solution of fluorine atoms. The dislocation d_2 is eventually depinned before escaping the film surface. In the meantime, a third dislocation, d_3, is nucleated. A total of 10 dislocations were emitted over 7 min. The stress required to activate this intergranular source can be qualita-

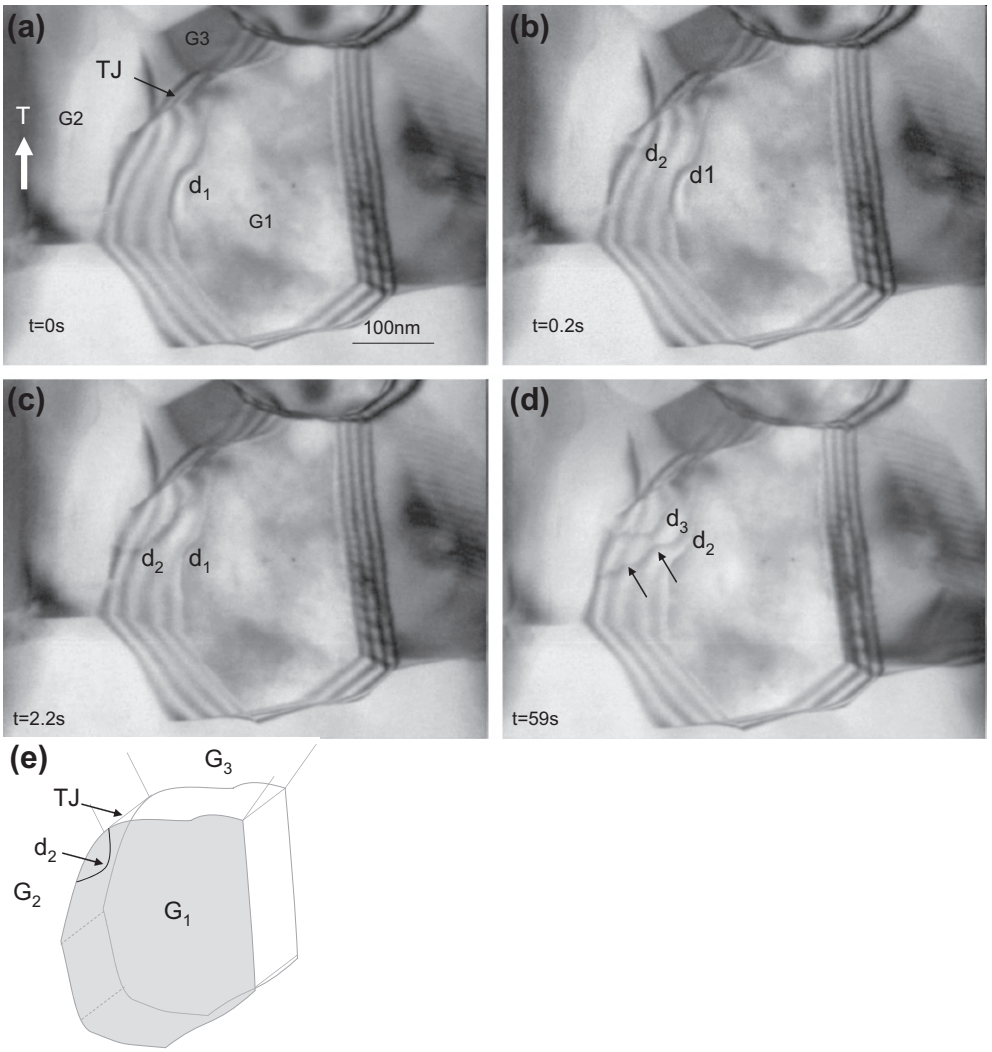

Fig. 3. (a)–(d) Intergranular dislocation activity monitored by in situ TEM at the onset of plasticity. Dislocations d_1–d_3 are nucleated close to the triple junction *TJ*123 and propagate at the *GB*12 interface. (e) Sketch of the configuration of grains *G*1, *G*2, *G*3 and interfacial dislocation (see text for details).

tively estimated through the dislocation line tension just before the dislocation is emitted in the GB, i.e. in Fig. 3b. Fig. 4a shows the image of *GB*12 projected onto the GB plane. The dislocation d_2 is curved due to the local imposed resolved shear stress and its shape can be approximately fitted with a circle of a radius $R_s = 13$ nm. Although neither the Burgers vector of the dislocation nor its character is known, an upper bound for the resolved shear stress τ_s acting on the dislocation can be roughly estimated by the formula $\tau_s = \mu b/R_s$. Taking $\mu = 25.5$ GPa, $b = 0.29$ nm

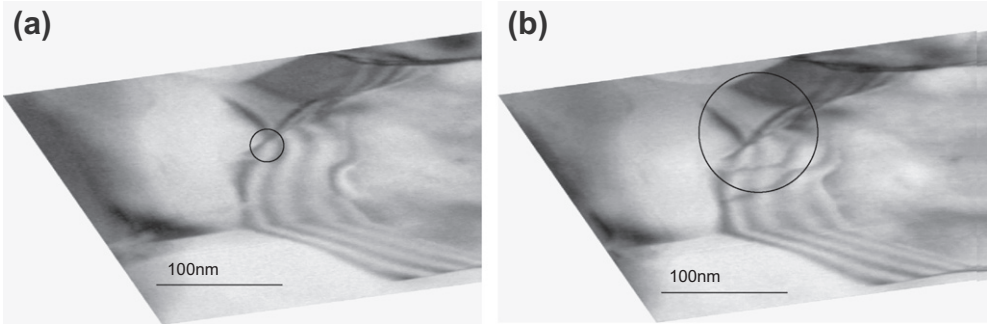

Fig. 4. Projection of the moving interfacial dislocation of Fig. 3 onto its habit plane in order to measure the curvature. The radius of curvature is inversely proportional to the local shear stress (see text for details).

Table 1
Characteristics of GBs where moving interfacial dislocations have been observed.

Misorientation axis	Misorientation angle (°)	CSL	Comments
$[\bar{1}\bar{1}\,1\,1]$	41.7	Σ9	Deviation 3.8°
$[6\bar{1}\,4\,7]$	48.6	–	HAGB
$[1\,2\,\bar{2}\,7]$	14.9	–	LAGB
$[\bar{1}\,5\,\bar{4}\,9]$	26.7	–	HAGB
$[21\,20\,\bar{9}]$	52.6	–	HAGB
$[4\,\bar{1}\,\bar{1}\,9]$	57.3	–	HAGB
$[19\,\bar{1}\,3\,3]$	52.6	–	HAGB
$[3\,\bar{1}\,\bar{1}\,10]$	12.7	–	LAGB
$[10\,6\,9]$	23.3	–	HAGB
$[13\,4\,6]$	19.1	–	HAGB
$[23\,0\,\bar{1}\,0]$	42.9	–	HAGB
$[4\,3\,19]$	18.2	–	HAGB
$[19\,14\,\bar{1}\,5]$	58.6	Σ3	Deviation 7.6°
$[\bar{1}\,3\,0\,0]$	44.5	Σ29	Deviation 1.6°
$[15\,\bar{3}\,16]$	58.9	–	HAGB

leads to $\tau_s \approx 500$ MPa, which is of the same order of magnitude as the flow stress measured at 2% strain in films of the same thickness [46]. The same type of measurements can be performed in order to estimate the stress needed to overcome the pinning points seen on Fig. 3d. Fig. 4b shows that the dislocation between two pinning points can be fitted by a circle of radius $R_p = 47$ nm. This leads to a stress $\tau_p = \mu b/R_p \approx 157 MPa$ which is much smaller than the stress required for operation of the source. This result indicates that GB source activation controls the onset of plastic deformation.

A total of 15 GB sources have been observed. The GB misorientation axis and angle are reported in Table 1. CSL GBs are defined according to the Brandon criterion [47], i.e. when the misorientation angle deviates from the exact value by less than $\Delta\theta = 15°/\sqrt{\Sigma}$. The proportion of the three types of active GB, i.e. 67% for HAGBs, 20% for CSL GBs and 13% for LAGBs is comparable to the proportion of these three types of GB observed in the initial microstructure. This result indicates that no particular type of GB is required to activate this intergranular deformation process.

3.3. Intergranular to intragranular transition and fracture

Upon further straining, i.e. above 2% strain, intragranular plasticity is detected in the larger grains. Fig. 5 shows a source (S) operating at *GB*12 (marked by a dashed line in Fig. 5a). The emitted dislocations of Burgers vector $1/2[1\,\bar{1}\,0]$, noted *d*, glide inside the grain in the $(\bar{1}\,1\,1)$ plane before being absorbed in the opposite *GB*23 (Fig. 5c). The stress needed to operate the source was estimated as described above and shown in Fig. 4, yielding a value of $\tau \approx 400$ MPa, which is close to the value obtained above.

When focusing on the source itself (Fig. 6), it can be noted that it is located in a defected area where the *GB*12 is distorted. Dislocation movement in the GB can be

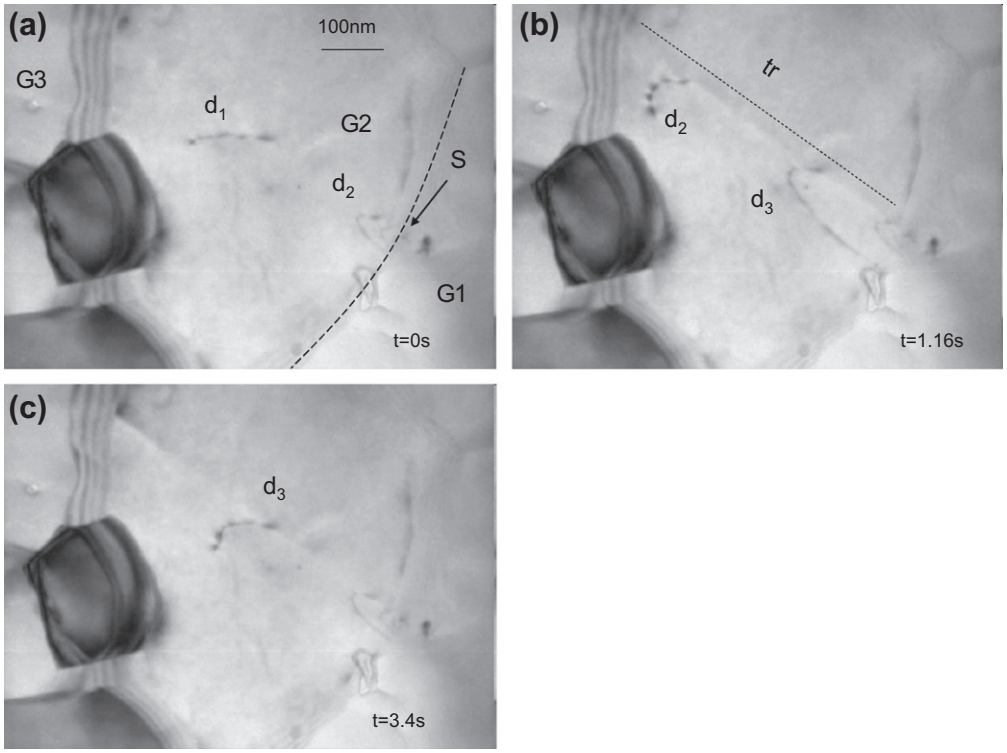

Fig. 5. Intragranular dislocation activity occurring above 2% total strain during in situ TEM straining. The sequence (a)–(c) shows a source S, located in the grain boundary *GB*12 (marked by a dashed line) emitting intragranular dislocations d_{1-3} in the plane delimited by its trace *tr* towards the interface *GB*23.

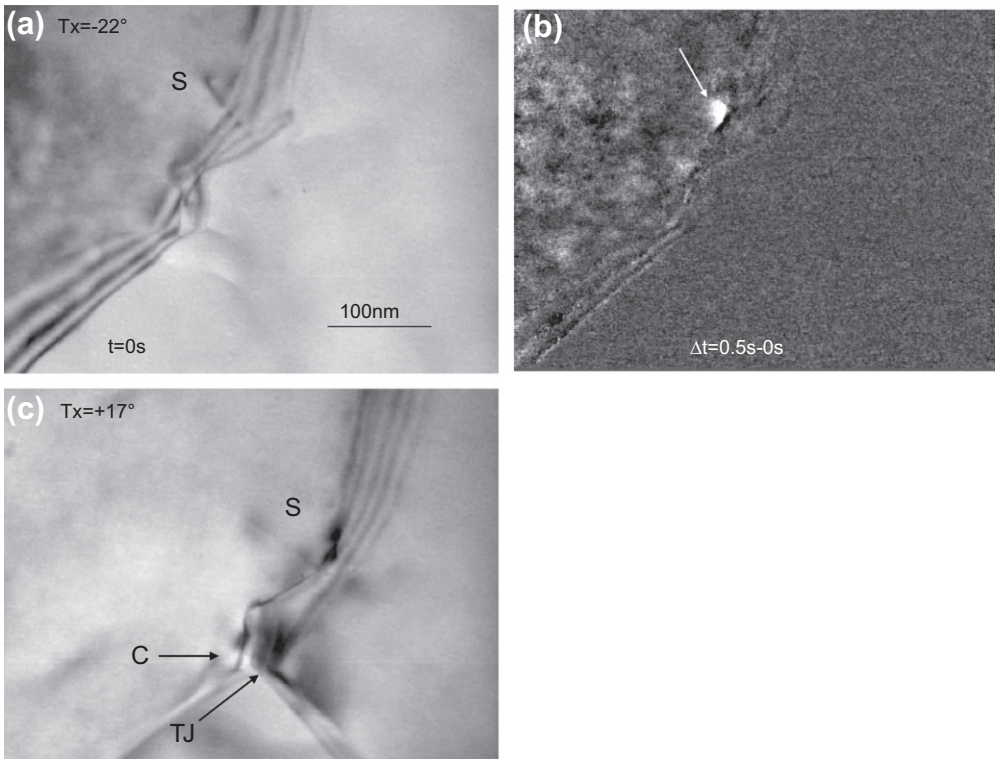

Fig. 6. Source S of Fig. 5 seen under different tilting conditions at the interface *GB*12. (a) Grain 2 in contrast. (c) Grain 1 in contrast. (b) Differential image obtained by subtracting a video screen capture before and after the emission of a dislocation by S. Note that S is located in a defected region of the grain boundary *GB*12.

observed although it is not as clear as in Fig. 3 due to the faint dislocation contrast. In Fig. 6b, an image difference between two images separated by 0.5 s is shown. The contrast is homogeneously grey in the two grains, indicating no change in the microstructure. However, a dark and bright contrast marked by an arrow is clearly visible in the *GB*12, highlighting the motion of a dislocation. This process is more clearly visible in the video sequence available in the Supplementary Material. It can thus be postulated that some plastic deformation carried in the interface is transferred in the grain interior when the glide of GB dislocations is perturbed in a defected area. A GB source can then form. Fig. 6a and c show the source area under two different inclination angles along the straining axis (the tilt axis is noted Tx). In Fig. 6c, a whiter area (noted *C*) at the triple junction (*TJ*) close to the source can be observed. This can be attributed to the early stage of cavitation and is probably the result of GB dislocation glide that cannot be accommodated at the triple junction.

At the same time, GB migration was also observed. Fig. 7 shows an example of the shrinkage of a grain in less than 1 min. This migration occurs after an increment in stress, confirming the existence of stress-coupled GB migration. As proposed in several models and computer simulations, we can suppose that this mechanism results also from the motion of GB dislocations [48–51]. Thus, GB dislocation activity can trigger stress-assisted grain growth. Because of the relatively isotropic elastic behavior of Al, the driving force due to strain energy difference amongst different grains is believed to be low [24]. However, due to the curvature of the GBs, capillarity forces are also involved in the process [52].

Fig. 8a shows a typical microstructure deformed by about 4%. The grain *G*1 is two times larger than the largest grains measured in the initial microstructure, which suggests that *G*1 has grown under stress in a process similar to the one depicted in Fig. 7. The high dislocation density in grain *G*1 indicates that intragranular plasticity fully develops after grain growth. Dislocations inside *G*1 were produced by the interactions of gliding dislocations in intersected planes originating from different GB sources. One such source, *S*, emitting one dislocation per second can be observed at *GB*13. Dislocations emitted from *S* are more clearly visible in a micrograph taken under a different inclination, as shown in the insert of Fig. 8a. These dislocations glide in the same plane, with a trace indicated with a dashed line, and form a pile-up which crosses the entire grain *G*1 and which stops against *GB*12. Fig. 8c shows *GB*12 under a different inclination.

In the region where the pile-up stops, the highly localized bending contours in *G*2 indicate that the crystal is severely distorted. This stress concentration region, *SC*, is able to promote dislocation nucleation in *G*2, though no dislocation activity, either nucleation or transmission, was observed. Dislocation motion in the *GB*12 can, however, be observed, suggesting that plasticity can be trans-

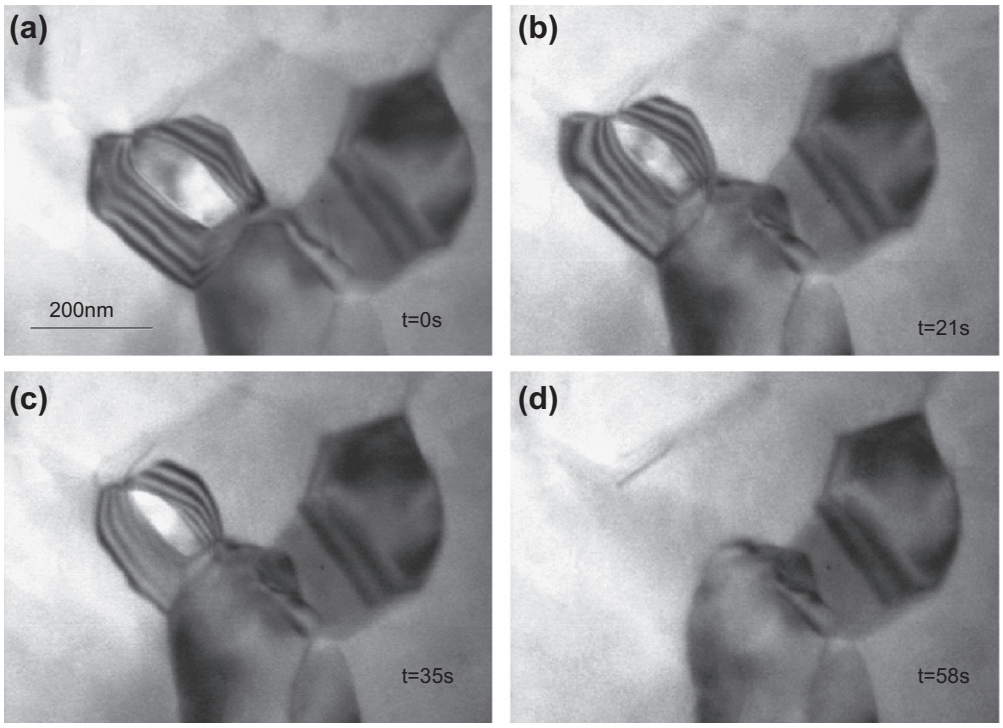

Fig. 7. Grain shrinkage and annihilation occurring after a stress increase. The annihilation of the smaller grains is triggered by stress-coupled GB migration, but also driven by surface tension reduction. This also leads to the growth of adjacent grains.

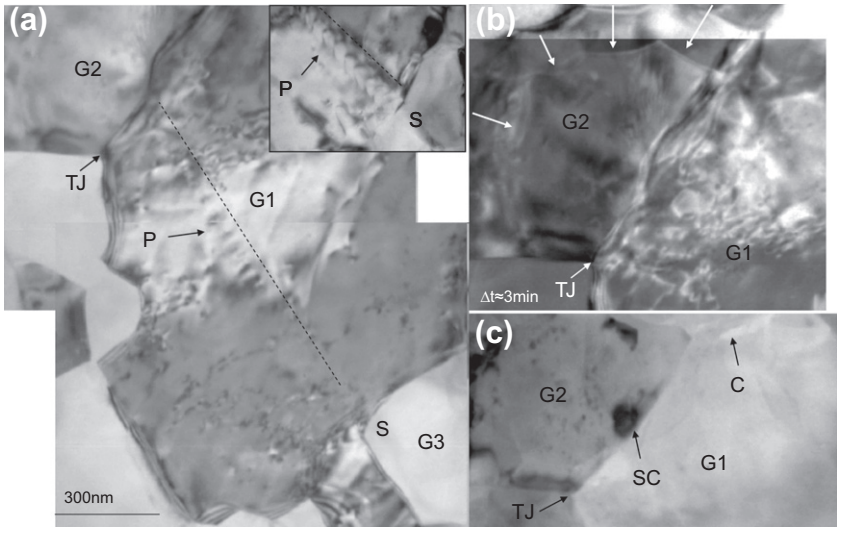

Fig. 8. Extensive intragranular dislocation activity occurring at about 4% total strain in a grain (*G*1) that has undergone significant growth. (a) Global view of the deformed grain *G*1, with the insert highlighting a dislocation pile-up *P* created by the source *S*. (b) Differential image before and after 3 min of dislocation activity in *G*1. (c) Micrograph of the same region but under a different orientation. Stress concentration (SC) and cavitation (C) initiation are visible.

fered back into the GB following a mechanism opposite to the one observed in Fig. 6. Fig. 8 shows an image difference between pictures taken within an interval of 3 min. While it shows strong bright and inhomogeneous contrasts in grain *G*1, indicating copious intergranular plasticity, no dislocation motion can be observed in *G*2. However, while the triple junction *TJ* remains fixed, the rest of the grain *G*2 has shrunk as indicated by the arrows. Nucleation and growth of cavities (*C*) has also been observed as shown in Fig. 8c. The cavities appear as thinner regions as already shown in Fig. 6.

The cavities can be clearly identified at lower magnification in Fig. 9, corresponding to one of the specimens shown in Fig. 1. They are located in the reduced section area of

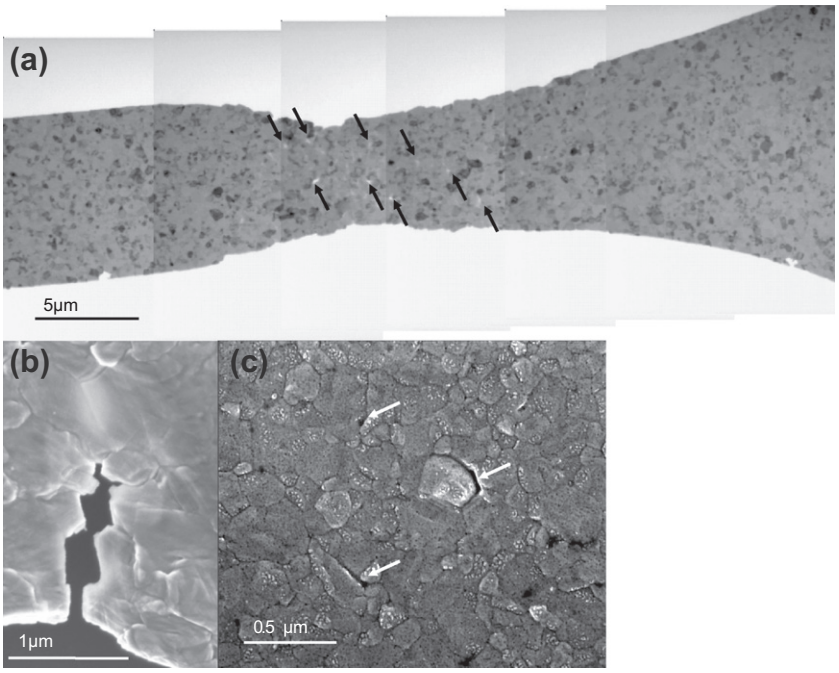

Fig. 9. (a) TEM micrograph showing necking and damage development in the necking region of a strained film. (b,c) SEM images showing the film roughness associated with the grain structure. (b) Growth of an intergranular crack. (c) Close up showing significant amount of grooving and intergranular porosity.

the film. This allows the film to deform extensively in this region, up to several tens of per cent. The cavities are located inside a necking region, and thus involve very large strains ($\geqslant$20%). These cavities eventually coalesce inside the film or, more frequently, a crack initiates on the film side and propagates from cavity to cavity along the GBs (Fig. 9b). This mechanism of ductile intergranular fracture is reminiscent of other GB ductile fracture observations in bulk metallic alloys in which the nucleation and growth of voids is favored at GBs, e.g. in Al alloys with precipitate-free zones near GBs [53,54].

Fig. 9c shows a SEM image of the initial microstructure. A large number of surface imperfections and porosities are indicated by white arrows. Atomic force microscopy images, not shown here, confirm the existence of grooves at least 10 nm deep. This local thickness reduction, which represents about 20 nm/300 nm = 7% of the film thickness, leads to significant stress concentration in particular areas. Although it is difficult to attribute these imperfections to emerging GBs, it can be supposed that a correlation exists between these imperfections and GB grooves. Hence, the existence of these imperfections may promote GB-mediated plasticity mechanisms.

4. Discussion

Fig. 10 summarizes the observations presented in the previous sections. In the early stage of plastic deformation, dislocation activity is primarily located at GBs (Fig. 10a). The activation of sources (S1) probably requires a high stress. However, as both numerical simulations and experimental observations suggest, the overall stress required to nucleate a dislocation from a free surface can be lowered by the presence of imperfections such as ledges [55,56]. For this reason, we suggest that stress concentration at GB grooves or surface imperfections can be sufficient to promote dislocation nucleation (see the insert in Fig. 10a). Although dislocation motion in GBs has already been observed by TEM [57,58,52], this mechanism is not often reported and there is no consensus as to how such dislocation sources can operate. It was also found that nucleation and propagation of interfacial dislocations is possible for all types of GBs independent of the misorientation. It is generally assumed that such dislocations are glissile in the GB plane if their Burgers vector is parallel to the GB interface and if the GB is perfectly flat [45]. In the case of curved interfaces, as observed in this study, the motion of these interfacial defects requires atomic rearrangements. The concomitant observation of GB migration under stress reveals also that diffusional processes are active. These processes are thought to occur over short distances because of the low temperature (0.3 T_m) [27].

At increasing strain, intragranular plasticity becomes active (Fig. 10b) owing to the operation of GB sources located at defects (S2). The nature of these defects may be intrinsic but they could be a consequence of intergranular plasticity itself. Indeed, because of the nonplanar motion of dislocations in the GB, dislocation ledges accumulate in specific locations, preventing further dislocation motion. Then, plastic deformation can be transferred into the grain interior from these regions. Because of the small grain size, intragranular dislocations are rapidly absorbed in the opposite GB. However, because of stress-assisted grain growth,

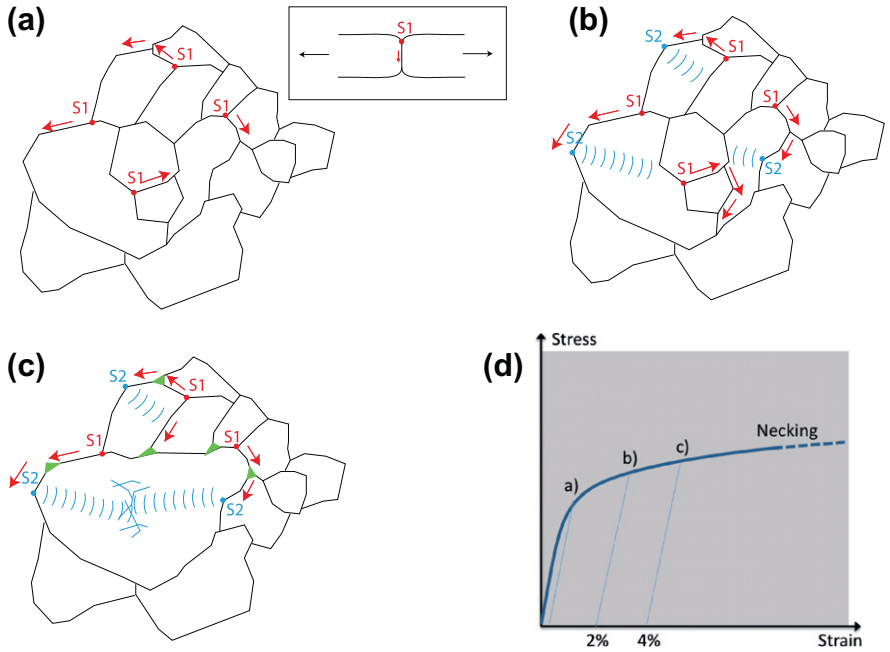

Fig. 10. Schematic of the sequential mechanisms involved in the plastic deformation of UFG Al films: (a) interfacial dislocation activity emitted from sources S1 leads to GB sliding (b) intragranular dislocation activity is triggered by sources S2 located in the GBs, and in parallel, stress-coupled GB migration leads to grain growth; (c) extensive plasticity and dislocation interaction starts to settle in grains that have undergone significant growth. Cavitation occurs at triple junctions when strain incompatibilities cannot be accommodated by dislocations. (d) Sketch of the sequential occurrence of the three previous mechanisms on the stress–strain curve.

the probability of finding more than one GB source increases with increasing grain size. Under such conditions, dislocations emitted in larger grains can be trapped inside as a result of dislocation interactions between slip systems (Fig. 10c) or with debris left by cross-slip.

The motion of GB dislocation without GB migration is believed to produce GB sliding. Because GBs are favorably oriented perpendicular to the film plane, GB sliding is thought to be accommodated principally by in-plane deformation. Because of strain incompatibilities between the grains, these sliding events cause the formation of cavities (Fig. 10c). GB sliding is commonly observed during creep of fine-grained materials at high temperature [59]. Contrary to GB sliding operating at high temperature as an accommodation process of diffusional creep, GB sliding without long-range diffusion [60,61] has been proposed to explain the superplastic behavior of metallic-based materials with grain remaining equiaxed [62]. In hexagonal close-packed metals where the von Mises condition cannot be always satisfied, slip-induced GB sliding is thought to accommodate strain incompatibilities at ambient temperature [63–65]. In the present study, however, GB sliding is not the result of a necessary process to accommodate grain deformation. In slip-induced GB sliding, and also contrary to our findings, it was found that GB sliding decreases for low Σ GBs compared to general GBs [66]. From this, it can be assumed that the specific behavior of thin films is significantly affected by surface imperfections probably located where GBs emerge, which favors GB dislocation nucleation. There is a clear analogy with the observation of the glide of dislocations between a silicon substrate and a 200 nm thick copper film reported in Ref. [67]. According to the authors, this mechanism results from constraint diffusional creep [68]: under stress and at high temperature, GBs are pulled away by the diffusion at the film surface of atoms towards the GBs. This mechanism produces a wedge at the GBs from where dislocations can be emitted due to stress concentration. The idea that GB grooves act as a stress concentrator from where plasticity is enhanced is similar.

This conclusion is in agreement with the statistical study of failure of films showing a decrease in the ductility with increasing surface area and decreasing thickness [69]. For instance, in a very thin film, the depth of GB grooves can reach a significant fraction of the film thickness. The effect of these imperfections tends to be more severe on plastic properties when the film thickness decreases. One should remember that the presence of imperfections has a significant impact on the premature occurrence of necking or shear bands, sometimes well before the ideal uniform elongation predicted by the Considère criterion (e.g. [70]). Note, however, that two other mechanisms in thin films can balance this negative impact of a higher density of imperfections, i.e. the increased rate sensitivity of small grain size materials due to the increasing importance of thermally activated mechanisms which delay the onset of localization, and the possible stabilizing effect of strain gradient plasticity on necking development (e.g. [71,72]). The extremely high rate sensitivity of thin Al films has been repeatedly observed as a result of thermally activated GB migration [24]. Even with

1%Si, Al films do relax 25% of the stress at room temperature within a couple of hours [73]. The GB-related mechanisms described in this work involve small activation volumes and are highly thermally activated, which also explains why very stable necks can be formed owing to the stabilizing effect of the rate sensitivity (see Fig. 9).

5. Conclusions

In situ TEM tensile experiments have been carried out on UFG Al thin films. The various deformation mechanisms have been identified from the early stages of the plastic regime up to fracture. Several conclusions can be drawn from these observations:

- Intergranular plasticity takes place at small plastic strain. It consists of the nucleation and motion of dislocations inside GBs. This mechanism takes place in all types of GBs irrespective of the misorientation.
- At larger strains, deformation can be transferred inside the grain interior.
- GB migration occurs under stress and leads to grain growth. Standard intragranular plasticity eventually takes over in the larger grains.
- GB sliding and cavitation appear as a consequence of intergranular plasticity and strain incompatibilities.
- Intergranular plasticity is controlled by imperfections such as GB grooves rather than by the type of GB.
- GB plasticity mechanisms are supposed to occur with the help of local atomic rearrangements.

This study proves the existence of several important synergies or connections between the deformation mechanisms, some being already well known, and some being more original: GB sliding is assisted by intergranular dislocation glide; accumulation of intergranular dislocations leads at some point to the generation of intragranular dislocations; GB migration leads to the occurrence of larger grains, which in turns favors intragranular dislocation accumulation through the increased probability of dislocation sources in a single grain; GB sliding results in the nucleation of voids at triple junctions. This interrelated array of phenomena, competitions and couplings demonstrates that a multitude of scenarios are possible in the range of submicron grain sizes depending on minute details of the microstructure, composition and geometrical artefacts such as GB grooving.

Acknowledgements

The authors want to acknowledge the GDRI MECANO for support. This work was carried out in the framework of the IAP program of the Belgian State Federal Office for Scientific, Technical and Cultural Affairs, under Contract Nos. P7/21. The support of the Fonds Belge pour la Recherche dans l'Industrie et l'Agriculture (FRIA) for M.C. is also gratefully acknowledged.

Appendix A. Supplementary material

Supplementary data associated with this article can be found, in the online version, at http://dx.doi.org/10.1016/j.actamat.2012.09.051.

References

[1] Hall E. Proc Phys Soc 1951;B64:747.
[2] Petch NJ. J Iron Steel Inst 1953;174:25.
[3] Valiev R, Islamgaliev R, Alexandrov I. Prog Mater Sci 2000;45:103–89.
[4] Meyers MA, Mishra A, Benson DJ. Prog Mater Sci 2006;51:427.
[5] Koch C. J Mater Res 2007;42:1403–14.
[6] Masumura R, Hazzledine P, Pande C. Acta Mater 1998;46:4527–34.
[7] Kumar KS, Van Swygenhoven H, Suresh S. Acta Mater 2003;51:5774.
[8] Lasalmonie A, Strudel JL. J Mater Sci 1986;21:1837–52.
[9] Kocks U. Metal Trans 1970;1:1121.
[10] Ashby M. Philos Mag 1970;21:399.
[11] Thompson A, Baskes M, Flanagan W. Acta Metall 1973;21:1017.
[12] Fleck N, Hutchinson J. J Mech Phys Sol 1993;41:1825–57.
[13] Nix W, Gao H. J Mech Phys Sol 1998;46:411–25.
[14] Evans A, Hutchinson J. Acta Mater 2009;57:1675–88.
[15] Pande CS, Masumura RA, Armstrong RW. Nanostruct Mater 1993;2:323–31.
[16] Yu C, Kao P, Chang C. Acta Mater 2005;53:4019–28.
[17] Massart T, Pardoen T. Acta Mater 2010;58:5768–81.
[18] Van Swygenhoven H, Derlet PM, Froseth AG. Acta Mater 2006;54:1983.
[19] Esquivel E, Murr L. Mater Sci Eng A 2005;409:13–23.
[20] Zhu Y, Liao X, Wu X. Prog Mater Sci 2012;57:1–62.
[21] Ivanisenko Y, Kurmanaeva L, Weissmueller J, Yang K, Markmann J, Rsner H, et al. Acta Mater 2009;57:3391–401.
[22] Liu P, Mao S, Wang L, Han X, Zhang Z. Scripta Mater 2011;64:343–6.
[23] Zhang K, Weertman JR, Eastman JA. Appl Phys Lett 2005;87:061921.
[24] Gianola DS, Van Petegem S, Legros M, Brandstetter S, Van Swygenhoven H, Hemker KJ. Acta Mater 2006;54:2253–63.
[25] Legros M, Gianola DS, Hemker KJ. Acta Mater 2008;56:3380–93.
[26] Gorkaya T, Molodov DA, Gottstein G. Acta Mater 2009;57(18):5396–405.
[27] Mompiou F, Caillard D, Legros M. Acta Mater 2009;57:2198–209.
[28] Rupert T, Gianola D, Gan Y, Hemker K. Science 2009;326:1686–90.
[29] Mompiou F, Legros M, Caillard D. J Mater Sci 2011;46:4308–13.
[30] Gorkaya T, Molodov KD, Molodov DA, Gottstein G. Acta Mater 2011;59:5674–80.
[31] Legros M, Gianola DS, Motz C. MRS Bull 2010;35:354–60.
[32] Forwood C, Clarebrough L. Philos Mag A 1981;44:31–41.
[33] Couzinie J, Decamps B, Priester L. Int J Plast 2005;21:759–75.
[34] Chassagne M, Legros M, Rodney D. Acta Mater 2011;59:1456–63.
[35] Lagow B, Robertson I, Jouiad M, Lassila D, Lee T, Birnbaum H. Mater Sci Eng A – Struct Mater Prop Microstruct Process 2001;309:445–50.
[36] Caillard D, Couret A. Microsc Res Tech 2009;72:261–9.
[37] Mughrabi H, Hoppel HW, Kautz M. Scripta Mater 2004;51:807–12.
[38] Mompiou F, Caillard D, Legros M, Mughrabi H. Acta Mater 2012;60:3402–14.
[39] Lojkowski W, Kirchner H, Grabski M. Scr Metall 1977;11:1127.
[40] Cabie M, Gianola DS, Legros M. Microsc Res Tech 2009;72:270–83.
[41] Gravier S, Coulombier M, Safi A, Andre N, Boe A, Raskin JP, et al. J Microelectromech Syst 2009;18/3:555–69.
[42] Colla MS, Wang B, Idrissi H, Schryvers N, Raskin JP, Pardoen T. Acta Mater 2012;60(4):1795–806.
[43] Thompson C. Annu Rev Mater Sci 2000;30:159–90.

[44] Lita A, Sanchez J. J Appl Phys 1999;85:876–82.
[45] Sutton AP, Baluffi RW. Interfaces in crystalline materials. Oxford: Oxford University Press; 1995.
[46] Haque M, Saif M. Exp Mech 2003;43:248–55.
[47] Brandon DG. Acta Metall 1966;14:1479.
[48] Cahn JW, Taylor JE. Acta Mater 2004;52:4887–98.
[49] Cahn JW, Mishin Y, Suzuki A. Acta Mater 2006;54:4953–75.
[50] Caillard D, Legros M, Mompiou F. Acta Mater 2009;57:2390–402.
[51] Mompiou F, Legros M, Caillard D. Acta Mater 2010;58:3676–89.
[52] Mompiou F, Legros M, Radetic T, Dahmen U, Gianola D, Hemker K. Acta Mater 2012;60:2209–18.
[53] Pardoen T, Dumont D, Deschamps A, Brechet Y. J Mech Phys Sol 2003;51:637–65.
[54] Pardoen T, Scheyvaerts F, Simar A, Tekoglu C, Onck P. Comptes Rendus Phys 2010;11:326–45.
[55] Godet J, Brochard S, Pizzagalli L, Beauchamp P, M SJ. Phys Rev B 2006;73:092105.
[56] Navarro V, Rodriguez de la Fuente O, Mascaraque A, Rojo JM. Phys Rev Lett 2008;100:105504.
[57] Kegg G, Horton C, Silcock J. Philos Mag 1973;27:1041.
[58] Mori T, Tangri K. Metal Trans 1979;10:733.
[59] Ruano O, Wadsworth J, Sherby O. Acta Mater 2003;51:3617–34.
[60] Ball A, Hutchinson MM. Metal Sci J 1969;3:1.
[61] Gifkins R. Metall Trans 1976;7A:1225.
[62] Sherby O, Wadsworth J. Prog Mater Sci 1989;33:169.
[63] Valiev R, Kaibyshev O. Phys Status Solidi A 1977;44:477–84.
[64] Mussot P, Rey C, Zaoui A. Res Mech 1985;14:69.
[65] Matsunaga T, Kameyama T, Ueda S, Sato E. Philos Mag 2010;90:4041–54.
[66] Watanabe T, Yamada M, Karashima S, Shima S. Philos Mag A 1979;40:667–83.
[67] Balk TJ, Dehm G. Artz Acta Mater 2003;51:4471–85.
[68] Gao H, Zhang L, Niw W, Thompson C, Artz E. Acta Mater 1999;47:2865–78.
[69] Coulombier M, Boe A, Brugger C, Raskin J, Pardoen T. Scripta Mater 2010;62:742–5.
[70] Hutchinson J, Neale K. Acta Metall 1977;25:839–46.
[71] Niordson C, Tvergaard V. Int J Solid Struct 2005;42:2559–73.
[72] Brugger C, Coulombier M, Massart TJ, Raskin JP, Pardoen T. Acta Mater 2010;58:4940–9.
[73] Coulombier M, Guisbiers G, Colla MS, Raskin JP, Pardoen T. Rev Sci Instrum, in press.